



**Lomonosov Moscow
State University**

X-ray Cross-Correlation Analysis of Mesocrystals

Elizaveta Morozova

Lomonosov Moscow State University, Faculty of Physics, Moscow, Russia

Supervisors: Nastasia Mukharamova, Ivan Vartaniants

DESY, Hamburg, Germany

ABSTRACT

X-ray Cross-Correlation Analysis (XCCA) was employed to evaluate the crystalline structure of mesocrystals consisting of the lead sulfide nanocrystals linked with organic ligands. The superlattice was shown to have a body-centered tetragonal structure, both by means of XCCA analysis and by the XCCA simulations of the anticipated structure.

Contents

ABSTRACT	0
INTRODUCTION	2
METHODS	3
X-RAY CROSS-CORRELATION ANALYSIS	4
RESULTS	6
SPATIALLY RESOLVED DIFFRACTION MAPS	8
X-RAY CROSS-CORRELATION ANALYSIS	12
CCF MODELING	13
CONCLUSION	15
REFERENCES	16

INTRODUCTION

Mesocrystals (MC) are three-dimensional arrays of iso-oriented single-crystalline particles with an individual size between 1 and 1000 nm [1]. Their physical properties depend on structural coherence determined by angular correlation between superlattice of nanocrystals (NC) and the underlying atomic lattice. Colloidal NCs stabilized by organic surfactants have been shown to be excellent building blocks for synthetic MCs with tailored structural properties. These are obtained by self-assembly of NCs from solution on a solid or liquid substrate by exploiting ligand–ligand interactions as reported in [2, 3]. Typically, ligands consist of wide-gap, bulky hydrocarbons which render the MCs insulating. In this work the MCs were synthesized using lead sulfide (PbS) NCs (shown in Fig. 1a) stabilized by Cu4Pac molecules forming a superlattice similar to the one shown in Fig. 1b.

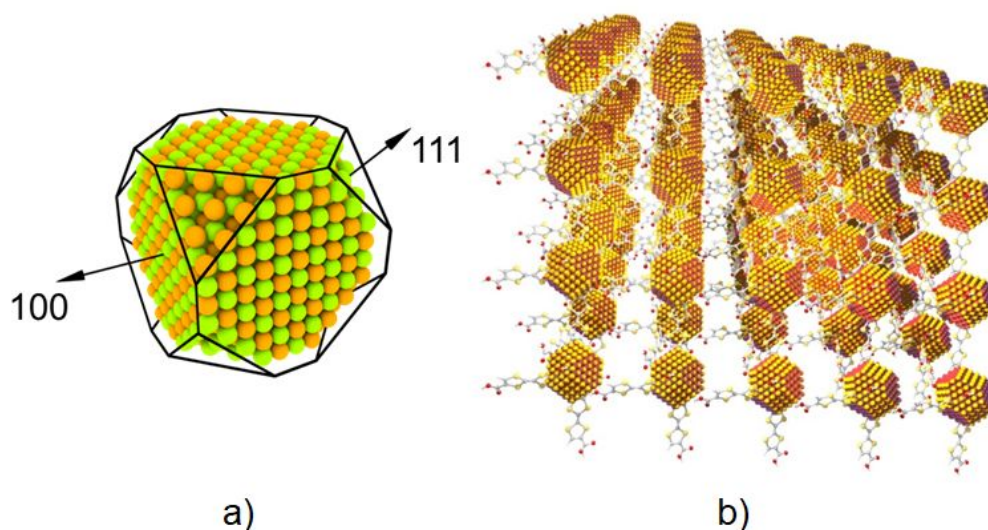


Figure 1. a) Schematic picture of lead sulfate (PbS) crystal forming the superlattice. b) The scheme of mesocrystal with the PbS as the lattice sites and organic ligands as bindings between them.

For X-ray experiments, the MCs were grown on a 500 μm x 500 μm X-ray transparent window consisting of a 50 nm thick Si_3N_4 membrane.

METHODS

The X-ray diffraction experiment was performed at the Coherence Beamline P10 of the PETRA III synchrotron source at DESY. The nanodiffraction endstation GINIX [4] was used to focus an X-ray beam with energy $E = 13.8$ keV ($\lambda = 0.898$ Å) down to 400×400 nm² size with KB-mirrors. The depth of the X-ray focus was about 0.5 mm. The sample was positioned perpendicular to the incoming X-ray beam as shown in Fig. 2. Two areas of the sample were scanned to analyze the spatial variations of the samples' structure. Within the first scanning region 441 diffraction patterns were collected on the 21×21 raster grid with a ~ 1 μm step size in both directions perpendicular to the incident beam. Within the second region 3721 diffraction patterns were obtained on the 61×61 raster grid. Each diffraction pattern was collected with an exposure time of 0.5 s to prevent radiation damage, which was assessed by repeating the scanning procedure several times on the same position of the sample. A two-dimensional detector (2070×2167 pixels with 75×75 μm² size) was positioned downstream at a distance of 38 cm from the sample and shifted so to have transmitted beam close to a corner (as shown in Fig. 2). With this geometry, we were able to detect the scattering signal from the MC SL as well as from PbS AL simultaneously and only a part of reciprocal space in wide angle scattering was accessible. Then the measured signal was corrected for background scattering. An example of the measured diffraction patterns is shown in Fig. 3 where both WAXS and SAXS (in inset) regions are visible.

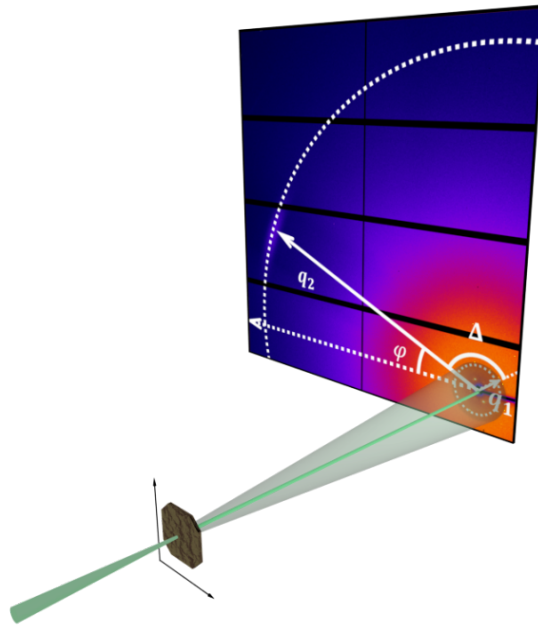


Figure 2. Scheme of the experiment. Incident beam was perpendicular to the sample surface. Detector was placed 38 cm from the sample. The shift to the corner of the detector allows registering both SAXS and WAXS reflections.

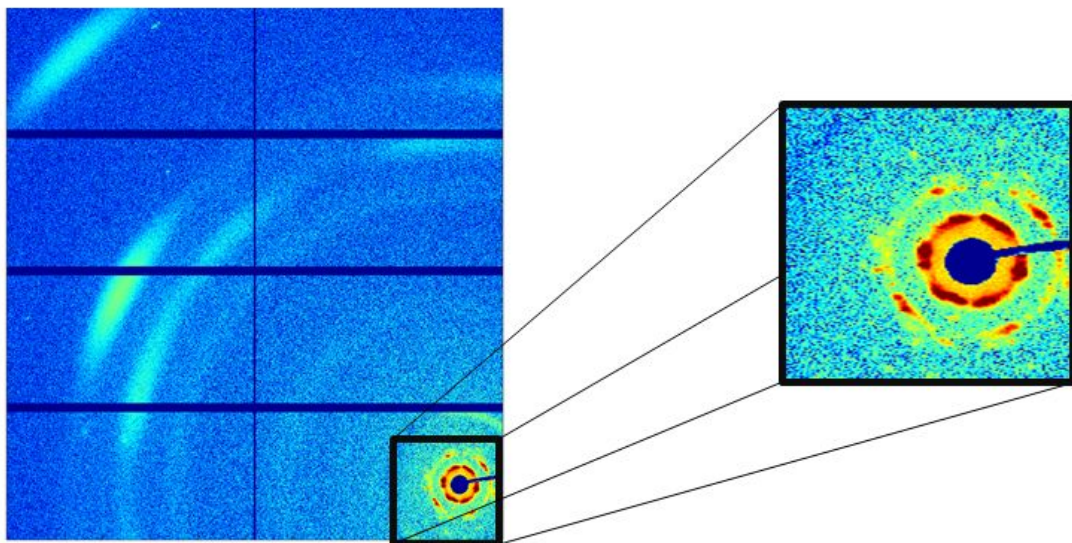


Figure 3. Typical diffraction patterns of the MC. WAXS peaks are considerably far from the center of the diffraction pattern so the only visible ones are in the range of angles $(\pi/2, \pi)$. SAXS peaks are located around the beamstop.

X-RAY CROSS-CORRELATION ANALYSIS

The XCCA method is widely used for the analysis of disordered or partially ordered systems such as colloids, liquid crystals, polymers etc. It provides information on angular correlations in the structure of molecules in the sample and on hidden symmetries and partial order of the system being studied. This method was also shown to be useful in the studying of mesocrystals [5].

While details and mathematical background on this method could be found e.g. in [6], main ideas are as follows. A two-point angular cross-correlation function (CCF) that can be calculated for each diffraction profile as

$$C(q_1, q_2, \Delta) = \frac{1}{2\pi} \int_{-\pi}^{\pi} I(q_1, \varphi) I(q_2, \varphi + \Delta) d\varphi \quad (1)$$

where $I(q, \varphi)$ is the intensity of diffraction pattern at the point with distance from the center of the pattern q and angular position φ . All the values used in this definition are shown in Fig. 4.

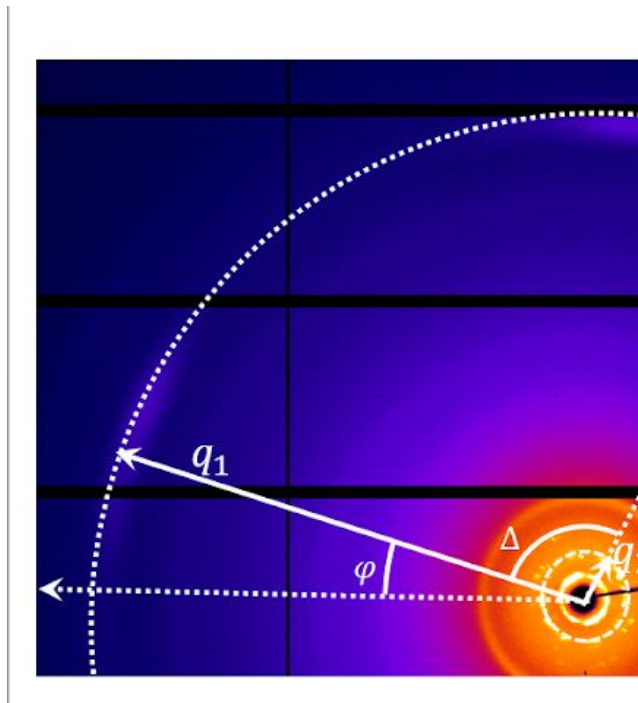


Figure 4. Graphical representation of variables used in the CCF definition. Arrows indicate the points of the diffraction patterns, in which the intensities are taken.

Experimentally obtained diffraction patterns contain defects such as detector gaps, beamstop, beamstop holder etc. In order to take into account their presence, we introduce into Eq. (1) the mask function

$$W(q, \varphi) = \{0, \text{gaps}, \text{beamstop}, \text{detector edges}\} \quad (2)$$

This gives us the final form of the CCF as in Eq. (3).

$$C(q_1, q_2, \Delta) = \frac{\int_{-\pi}^{\pi} I(q_1, \varphi)W(q_1, \varphi)I(q_2, \varphi+\Delta)W(q_2, \varphi+\Delta)d\varphi}{\int_{-\pi}^{\pi} W(q_1, \varphi)W(q_2, \varphi+\Delta)d\varphi} \quad (3)$$

Taking appropriate values of q_1 and q_2 we studied correlations between reflections in the WAXS and SAXS regions as well as autocorrelations in both regions. To obtain statistically meaningful data, CCFs were averaged over diffraction patterns from different points in the appropriate domain of the sample.

RESULTS

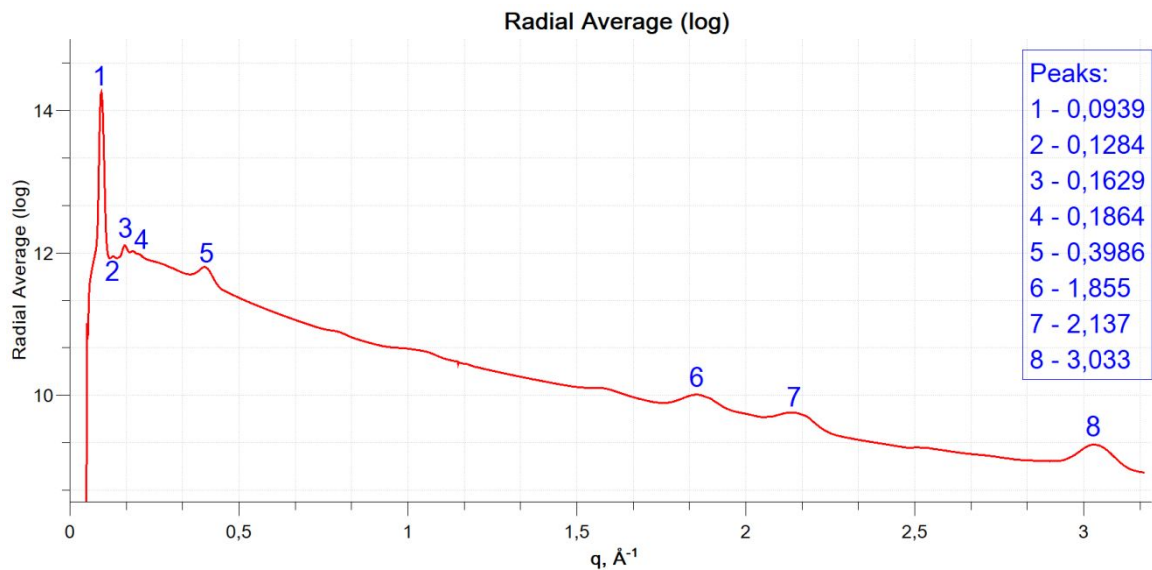


Figure 5. Graph represents the radial distribution of the intensity as summ of all diffraction patterns for the first area of the sample.

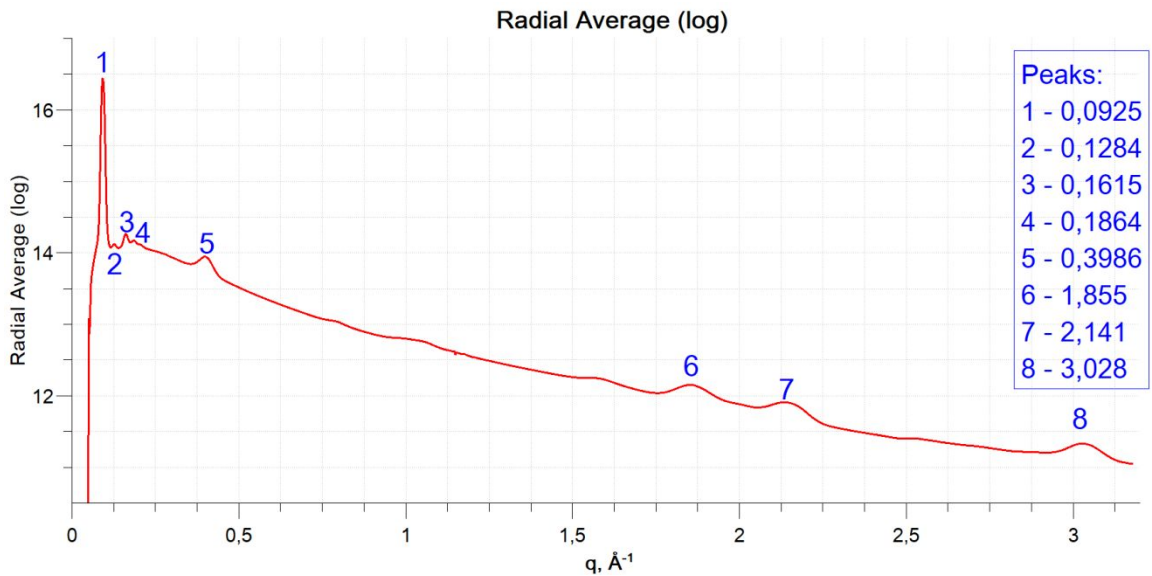


Figure 6. Graph represents the radial distribution of the intensity as sum of all diffraction patterns for the second area of the sample.

To investigate which peaks are contained in the diffraction patterns, we radially integrate scattered intensities for several lengths of the scattering vector with respect to the center of the incident beam. Resulting radial averages calculated for two different points of the sample are shown in Fig.5-6.

The WAXS region contains peaks at 1.9 , 2.14 and 3.03 \AA^{-1} , which correspond to $\{111\}$, $\{200\}/\{020\}/\{002\}$ and $\{022\}/\{220\}/\{202\}$ (Table 1) reflections of the PbS atomic lattice [7]. These values were used for finding the NC-containing area of the sample and later for obtaining spatially resolved maps of angular positions of the selected Bragg peaks in the diffraction patterns. Also those parameters let to calculate unit cell parameter for AL, $a=5,9\text{\AA}$.

We can resolve the two most intense peaks in the SAXS region with the momentum transfer values $q_1 = 0.09$ and $q_3 = 0.16 \text{ \AA}^{-1}$ and attribute them to the scattering of the superlattice (Table 2). As that comes from literature SL should be body-centered tetragonal lattice as at the Fig 7. Using the information about peak positions we calculated the unit cell parameters and tetragonal distortion. In our case $a=104 \text{ \AA}$, $c=135 \text{ \AA}$, $c/a=1,298$.

q (exp1)	q (exp2)	q(theory)	(hkl)	h+k+l
1,855	1,855	1,8436	111	3
2,137	2,141	2,1288	002/020/200	2

3,033	3,028	3,01	022/202/022	4
-------	-------	------	-------------	---

Table 1. Table contains data obtained from two areas of the sample and theoretical estimation of WAXS peak positions based on the miller indecies.

q (exp1)	q (exp2)	q(theory)	(hkl)	h+k+l
0,0939	0,0925	0,093	002	2
0,1284	0,1284	0,1263	112	4
0,1629	0,1615	0,1701	220	4
0,1864	0,1864	0,187	031/301	4

Table 2. Table contains data obtained from two areas of the sample and theoretical estimation of SAXS peak positions based on the miller indecies.

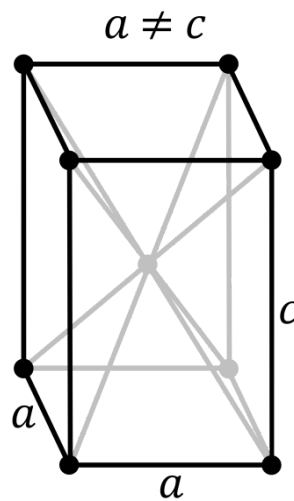


Figure 7. Scheme of body-centered tetragonal structure.

SPATIALLY RESOLVED DIFFRACTION MAPS

To find the NC-containing area of the sample, we evaluated the intensity of diffraction patterns in the WAXS and SAXS regions, corresponding to the scattering from the PbS atomic lattice. For each diffraction pattern we integrated the intensity in different regions. This way we create spatially resolved maps of the intensity, which are shown in as heat maps. As it's seen at Fig. 8 there are no domains or any structure.

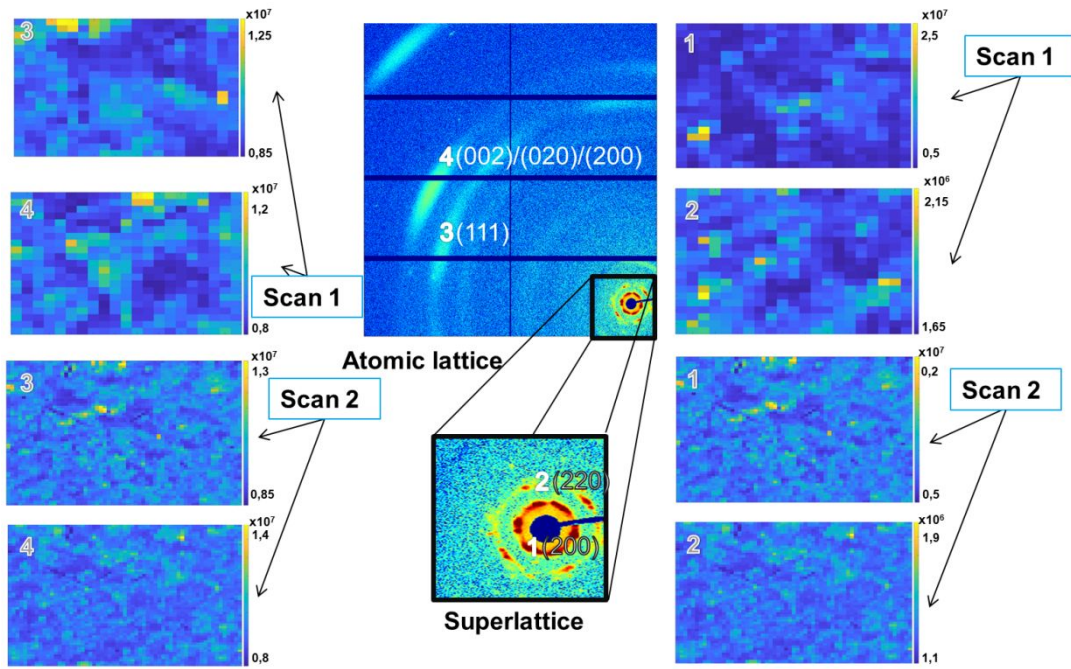


Figure 8. Spatially resolved maps for intensities of WAXS and SAXS for two scans of sample. No domains obtained.

To study the crystalline structure of the sample we found the positions of each peak in every point of the sample and marked these positions with lines from the center of beam. The length of every line corresponds to the intensity of the peak. As expected there are also no domains for both areas of the sample. There are some poorly organized regions but they can't be considered as domains due to their small size. (Fig 9-11.)

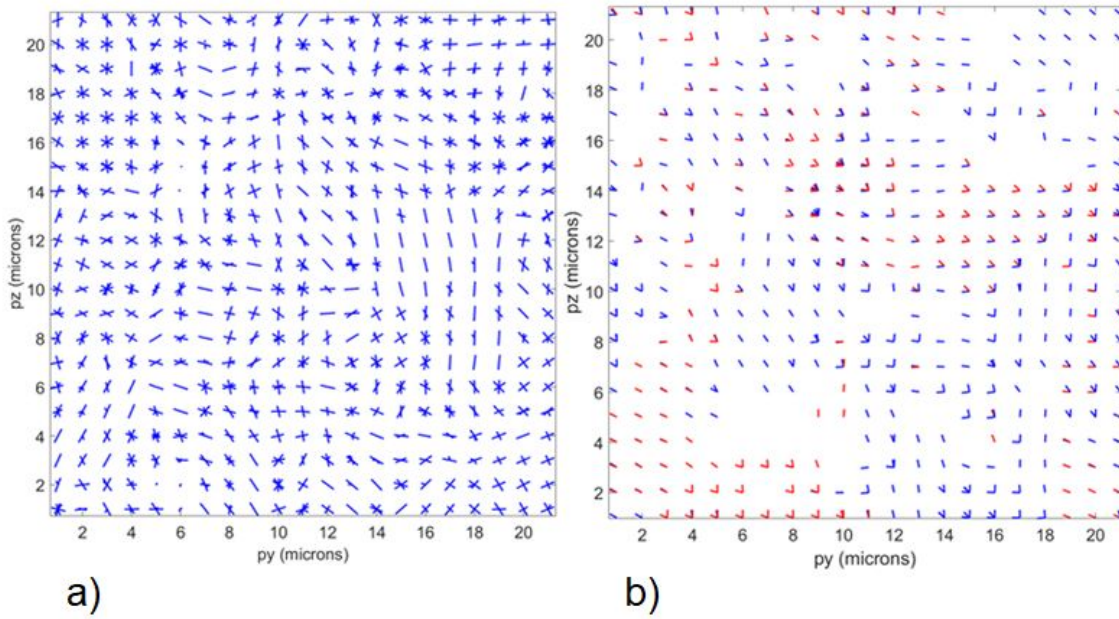


Figure 9. a) Positions of SAXS peaks from the first scan, lines correspond to peaks with q in the range $(0,9; 1,0) \text{ \AA}^{-1}$. b) Positions of WAXS peaks from the first scan. Blue lines correspond to peaks with q in the range $(2,0; 2,2) \text{ \AA}^{-1}$, red – to $(1,7; 1,9) \text{ \AA}^{-1}$.

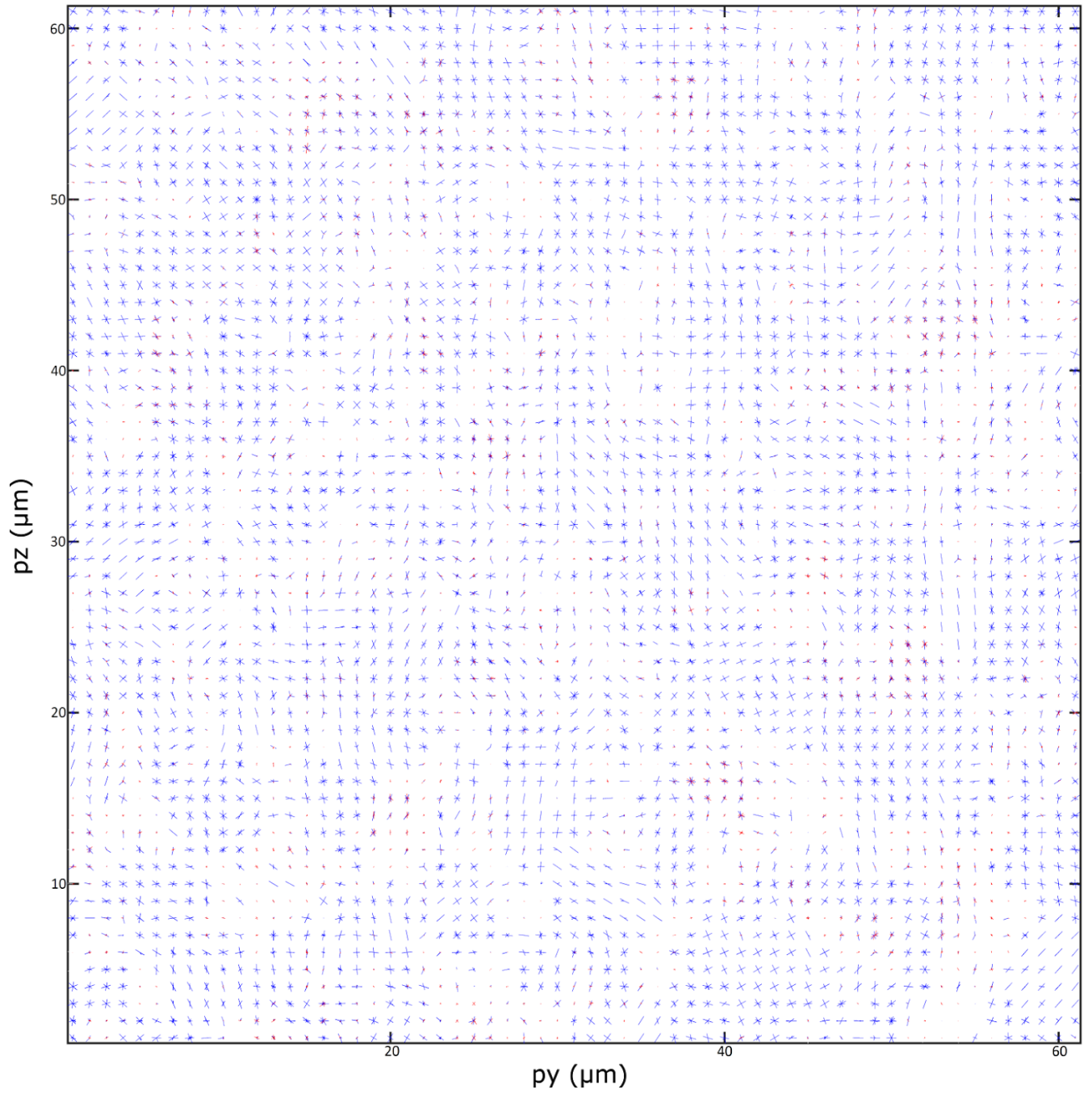


Figure 10. Positions of SAXS peaks from the second scan. Blue lines correspond to peaks with q in the range $(0,9; 1,0) \text{ \AA}^{-1}$, red – to $(0,12;0,13) \text{ \AA}^{-1}$.

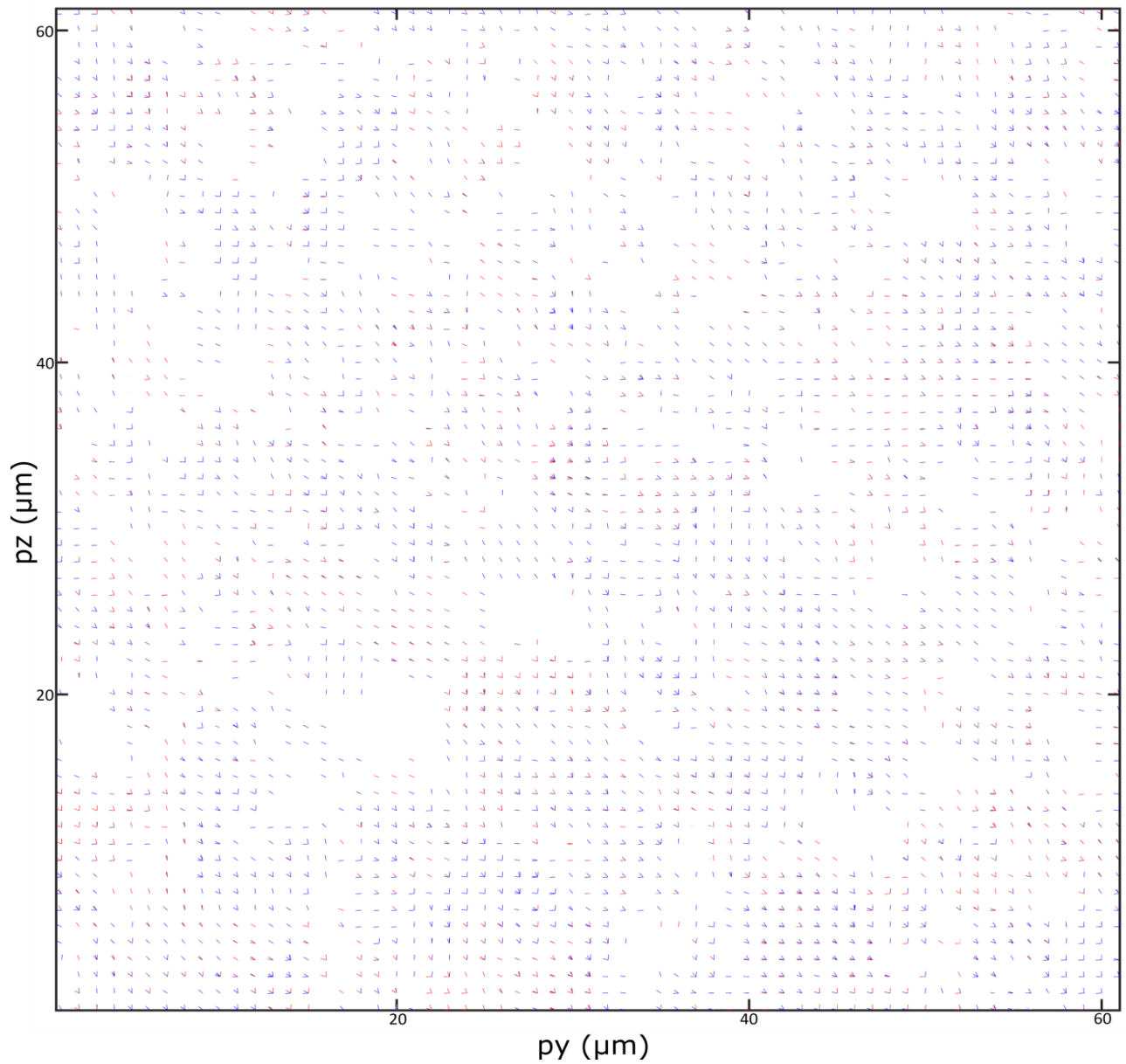


Figure 11. Positions of WAXS peaks from the second scan. Blue lines correspond to peaks with q in the range $(2,0; 2,2) \text{ \AA}^{-1}$, red – to $(1,7;1,9) \text{ \AA}^{-1}$.

To see how WAXS regions correlate with SAXS regions X-ray Cross-Correlation Analysis is need to be applied.

X-RAY CROSS-CORRELATION ANALYSIS

Here we calculate the CCF $C(q_1^{SL}, q_{200}^{AL}, \Delta)$ averaged over diffraction patterns. The resulting CCFs for both areas are shown in Fig. 12. One can observe four main peaks at $\Delta = \pm 45^\circ$ and $\pm 135^\circ$, representing the relative angles between q_1^{SL} and q_{200}^{AL} . The small peaks at $\Delta = \pm 90^\circ$ could be attributed to the reflections from parts of the sample with another orientation, partially illuminated by the considerably big incident beam.

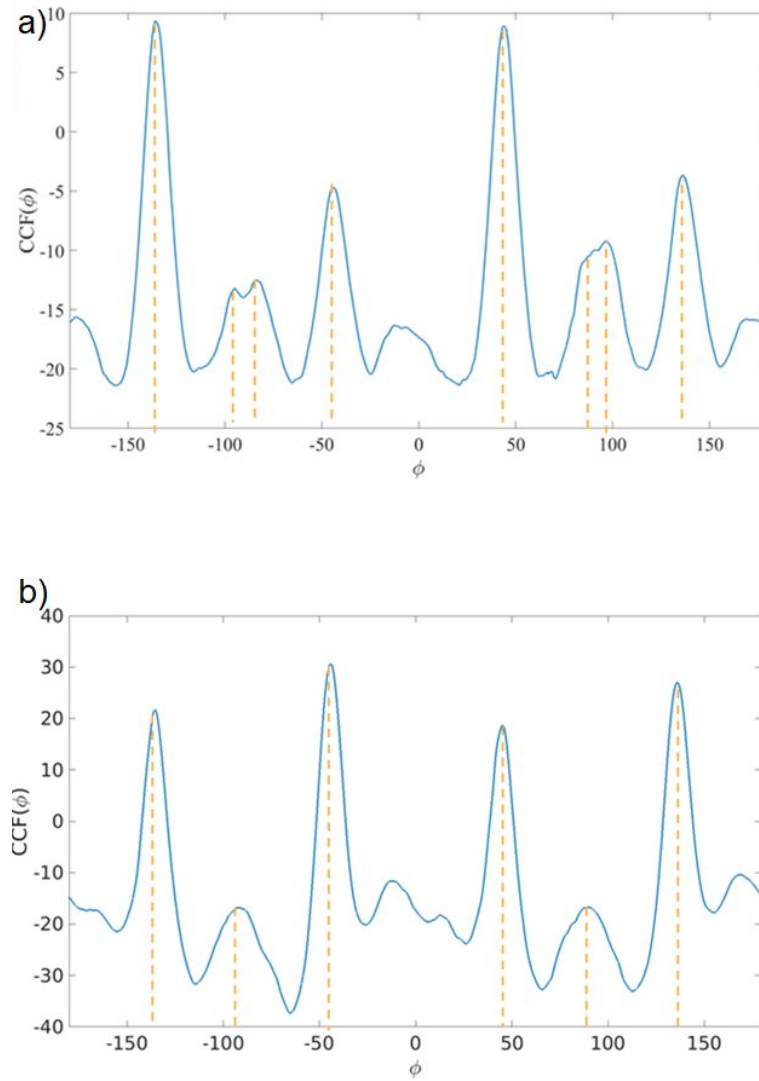


Figure 12. Cross-correlation functions for a) the first scan; b) the second scan. As it seen there are peaks at $\Delta = \pm 45^\circ$, $\pm 90^\circ$, $\pm 135^\circ$. Positions of peaks for both areas of sample looks similar as expected.

CCF MODELING

To create the CCF model we need to model the diffraction pattern from MC. We can assume that reciprocal space is a Fourier transformation of the normal space to model the diffraction patterns. The models we created are shown at the Fig. 13-14. They represent two typical structures the sample mostly consists of: tetragonal and hexagonal.

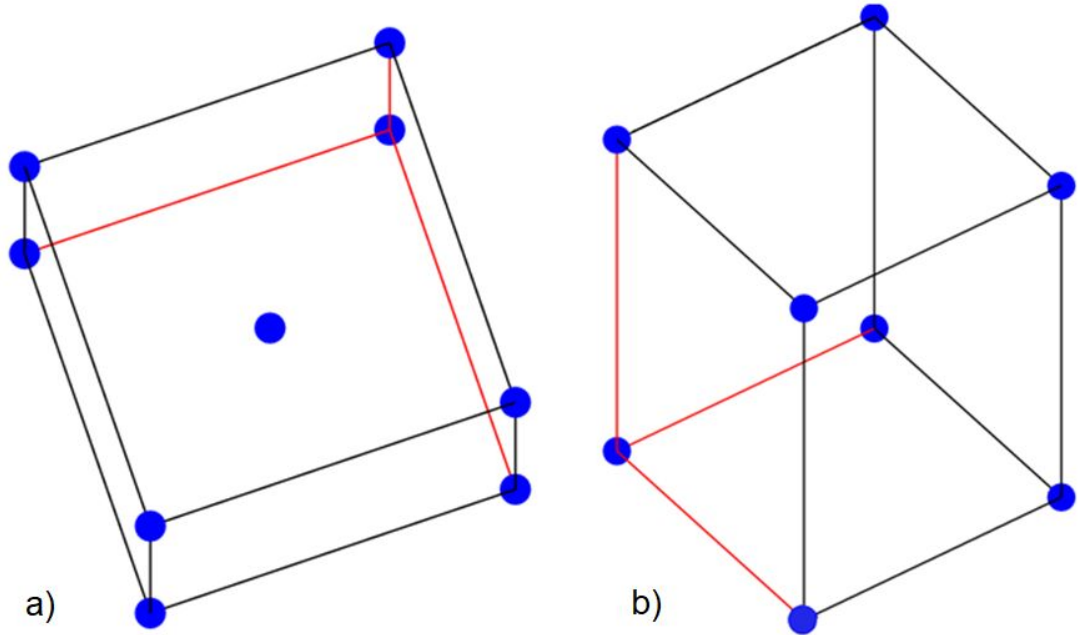


Figure 13. Orientations of typical structures the sample mostly consists of: a) tetragonal; b) hexagonal.

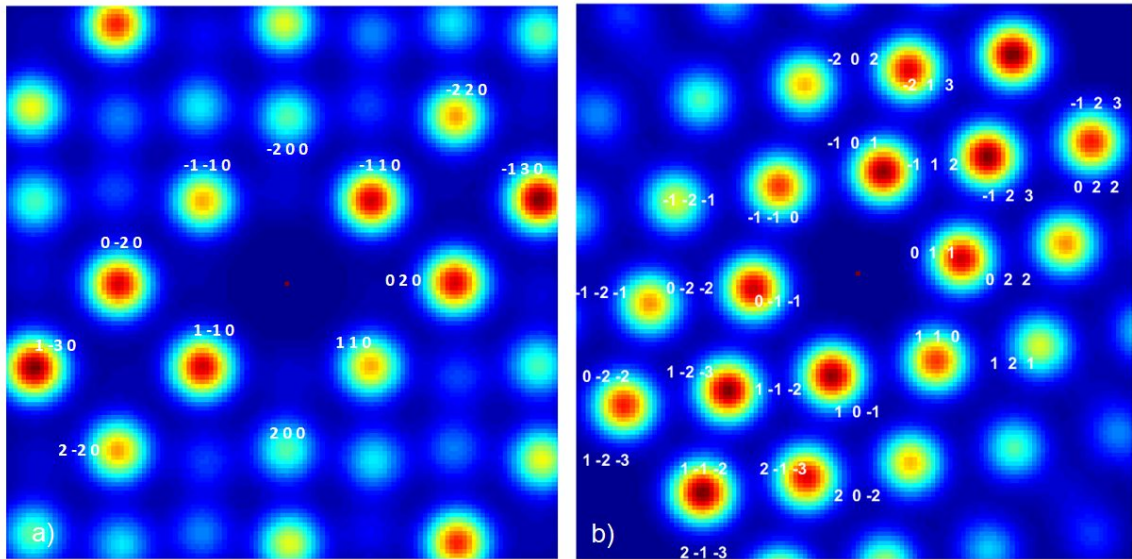


Figure 14. Models diffraction patterns formed with typical structures the sample mostly consists of: a) tetragonal; b) hexagonal.

To see that those models agree with the reality, we took two typical and most common diffraction patterns to nominate peaks on them (Fig. 15).

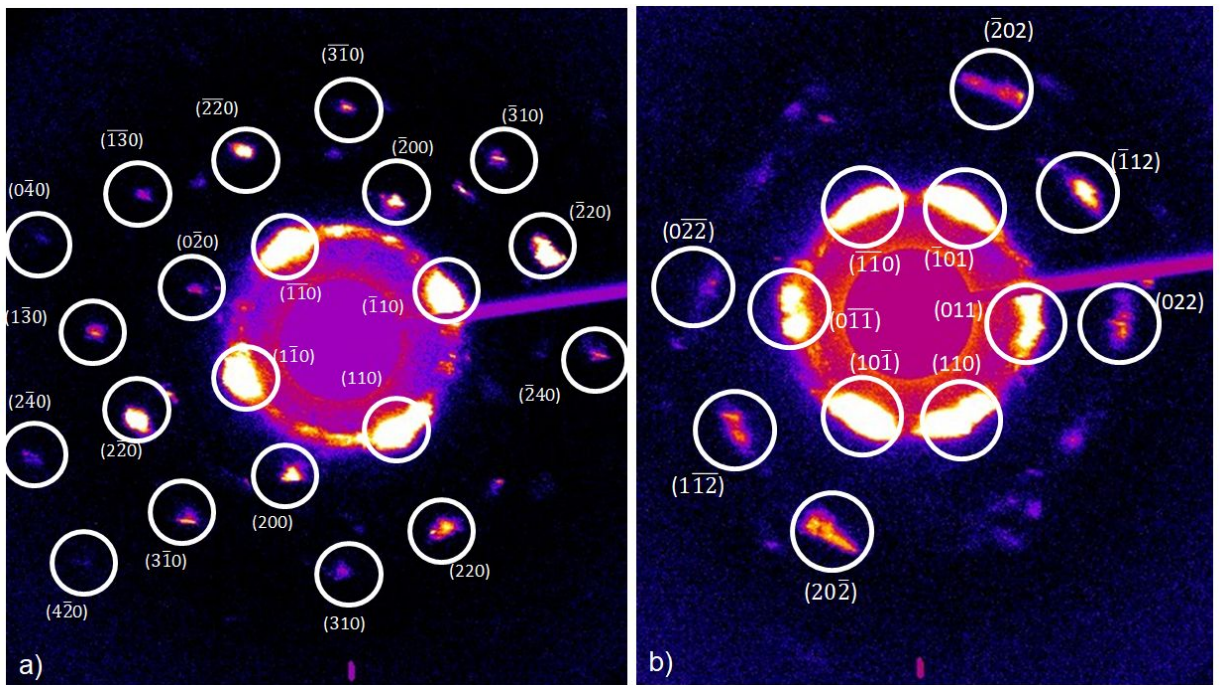


Figure 15. Two typical diffraction patterns that form the structure of: a) tetragonal; b) hexagonal;

The calculated CCF for the experimental data and model CCF for the first area of sample are shown in Fig. 16. Clearly, they are in a good agreement with each other, which indicates the fidelity of our evaluations of the unit cell distortion. Amplitudes of the peaks in the experimental curve are different because of the varied intensities of the original Bragg peaks in the diffraction patterns.

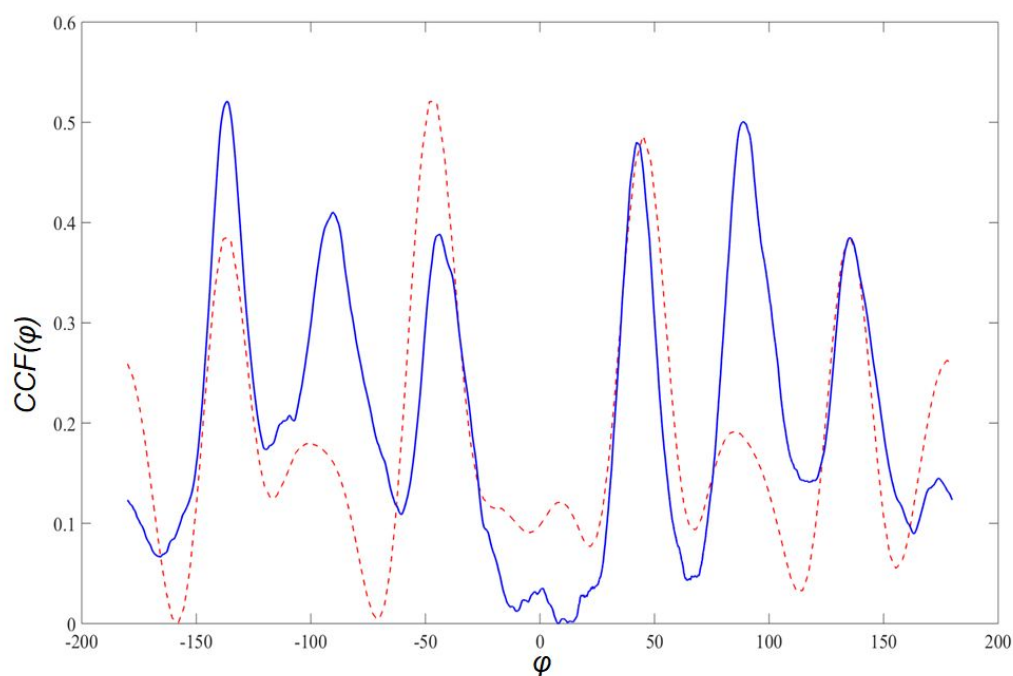


Figure 16. Comparison of real CCF and modeled CCF. Blue is the real one and the red one represents the model.

CONCLUSION

In this work we studied diffraction patterns of the MC consisted of PbS NCs and organic linkers. Spatially-resolved maps were obtained for the WAXS and SAXS regions of the collected diffraction patterns from two areas of the same sample. The sample was shown to contain no domains and chaotic structure. The unit cell structure of the SL was evaluated by the analysis of the diffraction patterns in the SAXS region. The MC was shown to have the body-centered tetragonal lattice with tetragonal distortion $c/a=1,298$. By the XCCA analysis, this structure was confirmed. Despite we cannot see any structure, XCCA shows that there are two preferable orientations of the lattice in the sample and in general the orientation between AL and SL is conserved.

REFERENCES

1. Song, Rui - Qi, and Helmut Cölfen. "Mesocrystals—ordered nanoparticle superstructures." *Advanced materials* 22.12 (2010): 1301-1330.
2. André, Alexander, et al. "Toward conductive mesocrystalline assemblies: PbS nanocrystals cross-linked with tetrathiafulvalene dicarboxylate." *Chemistry of Materials* 27.23 (2015): 8105-8115.
3. Boneschanscher, Mark P., et al. "Long-range orientation and atomic attachment of nanocrystals in 2D honeycomb superlattices." *Science* 344.6190 (2014): 1377-1380.
4. Salditt, Tim, et al. "Partially coherent nano-focused x-ray radiation characterized by Talbot interferometry." *Optics express* 19.10 (2011): 9656-9675.
5. Zaluzhnyy, Ivan, et al. "Quantifying Angular Correlations between the Atomic Lattice and Superlattice of Nanocrystals Assembled with Directional Linking." *Nano Letters* (2017).
6. Kurta, Ruslan, et al. "Structural Analysis by X-ray Intensity Angular Cross Correlations." In *Advances in Chemical Physics*, Volume 161; John Wiley & Sons, Inc. (2016): 1-39.
7. Gurin, V. S. "Nucleation and growth of PbS nanocrystals and simulation of X-ray diffraction patterns." *Journal of crystal growth* 191.1 (1998): 161-165.